Capillary self-alignment of polygonal chips: A generalization for the shift-restoring force

J. Berthier,[1] S. Mermoz,[2] K. Brakke,[3] L. Sanchez,[4] C. Frétigny,[5] and L. Di Cioccio[4]
[1)] *Biotechnology Department, CEA-Leti, 17 avenue des Martyrs, 38054 Grenoble, France*
[2)] *STMicroelectronics, 850 rue Jean Monnet, 38926 Crolles Cedex, France*
[3)] *Mathematics Department, Susquehana University, 514 University avenue, Selingrove, PA 17870, USA*
[4)] *Microelectronic Department, CEA-Leti, 17 avenue des Martyrs, 38054 Grenoble, France*
[5)] *ESPCI, 10 rue Vauquelin, 75005, Paris, France*

(Dated: 6 May 2012)

Capillary-driven self-alignment using droplets is currently extensively investigated for self-assembly and microassembly technology. In this technique, surface tension forces associated to capillary pinning create restoring forces and torques that tend to bring the moving part into alignment. So far, most studies have addressed the problem of square chip alignment on a dedicated patch of a wafer, aiming to achieve 3D microelectronics. In this work, we investigate the shift-restoring forces for more complex moving parts such as regular – convex and non-convex – polygons and regular polygons with regular polygonal cavities. A closed-form approximate expression is derived for each of these polygonal geometries; this expression agrees with the numerical results obtained with the Surface Evolver software. For small shifts, it is found that the restoring force does not depend on the shift direction or on the polygonal shape. In order to tackle the problem of microsystem packaging, an extension of the theory is done for polygonal shapes pierced with connection vias (channels) and a closed form of the shift-restoring force is derived for these geometries and again checked against the numerical model. In this case, the restoring force depends on the shift direction. Finally, a non-dimensional number, the shift number, is proposed that indicates the isotropic or anisotropic behavior of the chip according to the shift direction.

I. INTRODUCTION

Capillary-driven self-alignment using droplets, or capillary self-assembly (CSA), is currently extensively investigated for self-assembly and microassembly technology[1–8]. In this technique, surface tension forces associated to capillary pinning create restoring forces and torques that tend to bring the moving part into alignment. In the field of 3D microelectronics, the method aims to be an alternate approach to the "pick and place" approach. In the capillary technique, the chip is deposited on top of a water droplet and is brought into alignment by the action of capillary forces, because the liquid interface tends to minimize its free area[9]. After alignment, which is fast, evaporation brings the chip into contact with the pad on the wafer, and direct bonding is possible if the two surfaces are sufficiently hydrophilic[10–13]. It is expected that self-alignment methods could be faster and more precise than the conventional robotic method. Developments have been fast, and it has been found that a square chip can be aligned by the action of restoring forces and torques if a certain number of precautions are taken[14,15]. A review of the different concepts for 3D integration has recently been published by Lee and coworkers[16].

In parallel, following the pioneering work of the Whitesides group[17], new investigations have started: Knuesel and colleagues have used the method for the assembly of segmented monocrystalline solar cells[18], Avital and Zussman have developed CSA methods for fluidic assembly of optical components[19], Zhang and colleagues have investigated the CSA of drosophila embryos on 2-D arrays of hydrophobic sites on a silicon substrate in water[20], Stauth and Parviz have developed the self-assembly of single-crystal silicon circuits on plastic[21], and Fukushima and colleagues have studied the use of CSA for microsystem packaging[22]. These investigations are mainly experimental (except for the work of Zhang et al.).

In this work, we present a novel theoretical and numerical approach to the shift restoring forces for polygonal chips. For many different polygonal shapes, the shift restoring force is calculated analytically for an approximation, and numerically in more detail. In the particular case of regular polygons – convex or not – of the same perimeter, it is demonstrated that the magnitudes of the restoring forces at short range – small initial shift or at the end of the alignment process – are equal for all polygonal shapes. Also, the restoring force at small shift does not depend on the direction of the shift for these regular polygonal shapes. The theoretical results are in agreement with numerical results obtained with the Surface Evolver software[23]. Moreover, it is shown that the approach can be extended to polygonal chips with polygonal cavities, such as those used by Fukushima and coworkers to seal microsystems[22]. If connection vias or microchannels pierce the sides of the chip, the isotropic behavior is lost, and the former analytical expression has to be corrected by an anisotropic factor. Finally, it is shown that anisotropic chip geometries have restoring

forces different than regular shapes and the isotropicity is characterized by a non-dimensional number which we call the shift number.

II. THEORY

Consider a chip in shape of a polygon and a shift x in the direction as sketched in figure 1. Edge number k has length s_k and angle from horizontal θ_k.

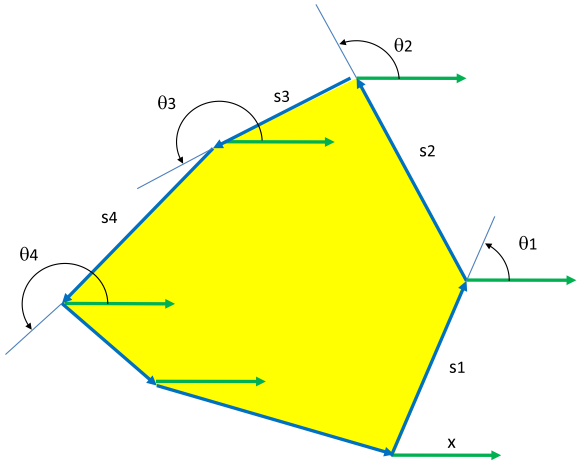

FIG. 1. Sketch of a polygon with shift direction.

Now consider the deformation of one edge of length s and angle θ, as shown in figure 2. The initial interface – assuming it is flat – has an area of

$$A_1 = sh, \tag{1}$$

where h is the height of the liquid layer. The surface energy is then

$$E_1 = \gamma A_1 = \gamma sh, \tag{2}$$

where γ is the surface tension. The shifted interface – still assuming it is flat – has an area of

$$A_2 = s\sqrt{h^2 + x^2 \sin^2\theta}, \tag{3}$$

where x is the shift. The corresponding surface energy is

$$E_2 = \gamma A_2 = \gamma s\sqrt{h^2 + x^2 \sin^2\theta}. \tag{4}$$

Note that an interface parallel to the direction of the shift keeps the same surface area ($\theta = 0$), and an interface perpendicular to the shift has the energy $E_2 = \gamma A_2 = \gamma s\sqrt{h^2 + x^2}$, which is what was found in our previous work in the case of a square chip and a shift perpendicular to an edge[9]. The restoring force corresponding to this single interface is

$$F = -\frac{\delta E_2}{\delta x} = -\gamma s x \sin^2\theta \frac{1}{\sqrt{h^2 + x^2 \sin^2\theta}}. \tag{5}$$

Approximating the surface energy of the whole interfacial area by the sum of the surface energy of all "facets" – i.e. not considering the inward curvature of the interface at the junction of two facets or any curvature in the middle of the face – the total surface energy after the shift is

$$E_2 = \sum_i E_i = \gamma A_2 = \gamma \sum_i s_i \sqrt{h^2 + x^2 \sin^2\theta_i}. \tag{6}$$

The restoring force is then

$$F = -\sum_i F_i = -\gamma x \sum_i s_i \sin^2\theta_i \frac{1}{\sqrt{h^2 + x^2 \sin^2\theta_i}}. \tag{7}$$

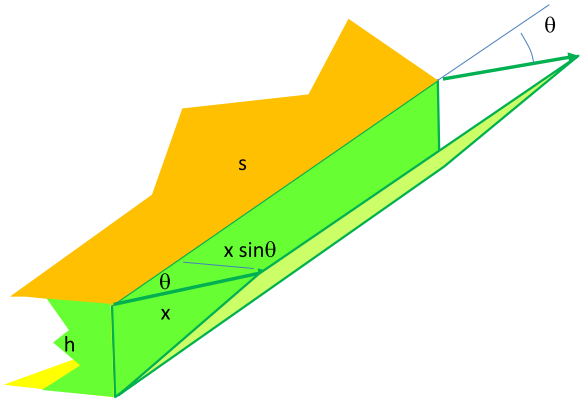

FIG. 2. sketch of a shifted interface.

An interesting observation is that, when x is very small in comparison with h, relation (7) collapses to

$$F = -\gamma \frac{x}{h} \sum_i s_i \sin^2\theta_i. \tag{8}$$

Relation (8) shows that when x is small, the restoring force is a linear function of x. On the other hand, if the shift is large compared to the vertical dimension of the fluid layer h, then (7) collapses to

$$F = -\text{sign}(x)\gamma \sum_i s_i |\sin\theta_i|. \tag{9}$$

In this last case, the restoring force is constant. If we apply relation (8) and (9) to the case of the square, we retrieve the relations given in previous work[9]. A geometrical interpretation of (9) is given in Appendix A.

Consider now polygons, convex or not, with equal edges. Then, for all i, we have $s_i = s$, and relation (8) becomes

$$F = -\gamma s \frac{x}{h} \sum_i \sin^2\theta_i. \tag{10}$$

Relation (10) can be simplified by introducing the polygon perimeter p and using the fact that the average of $\sin 2\theta$ over equally spaced angles is:

$$F = -\gamma \frac{x}{h} \frac{p}{2}, \tag{11}$$

where ϵ is the aspect ratio $2h/p$. An important remark is that the restoring force F at small range does not depend on the shift direction or on the shape of the polygon.

On the other hand, (9) becomes an asymptotic value for the shift restoring force for large shifts:

$$F = -\text{sign}(x)\gamma s \sum_i |\sin\theta_i|. \tag{12}$$

Note that the restoring force F in this latter expression depends on the polygonal shape and on the direction of the shift, but not on the magnitude of the shift. For a convex polygon, (12) is just the surface tension times twice the transverse width of the polygon, which is to be expected, since a large shift just stretches two horizontal surfaces, top and bottom, each of the width of the polygon.

III. REGULAR POLYGONS (CONVEX)

We investigate first the case of regular convex polygons. In Appendix B, it is shown that relation (12) for large shifts can be expressed by

$$F = -\frac{\gamma s}{2\sin\frac{\pi}{n}} \sum_i \left| \left[\cos\left(2(i+1)\frac{\pi}{n}\right) - \cos\left(2i\frac{\pi}{n}\right)\right]\sin\alpha + \left[\sin\left(2(i+1)\frac{\pi}{n}\right) - \sin\left(2i\frac{\pi}{n}\right)\right]\cos\alpha \right|, \tag{13}$$

where α is the shift angle. A non-dimensional expression for the force can be defined by

$$f = \frac{F}{\gamma p}. \tag{14}$$

And the asymptotic value of f – that we denote here the "shift number" Sf – is

$$Sf = \left|\frac{F}{\gamma p}\right| = -\frac{1}{2n\sin\frac{\pi}{n}} \sum_i \left| \left[\cos\left(2(i+1)\frac{\pi}{n}\right) - \cos\left(2i\frac{\pi}{n}\right)\right]\sin\alpha + \left[\sin\left(2(i+1)\frac{\pi}{n}\right) - \sin\left(2i\frac{\pi}{n}\right)\right]\cos\alpha \right|. \tag{15}$$

The shift number Sf depends only on the number of edges n, i.e. the polygonal shape, and the shift direction. It is a measure of the isotropic behavior of the chip. If Sf is invariant with α, the shift-restoring forces are isotropic. The shift numbers for 5 different regular polygons (equilateral triangle, square, pentagon, hexagon, and octagon) are shown in figure 3. The shift numbers are comprised between 0.5 and 0.7 in all cases. The square has the least isotropic behavior, with a maximum variation of the shift-restoring force of 30% with the shift direction; the other polygons show a variation of the shift-restoring force less than 15%.

In conclusion, the theory predicts that the free energy and restoring forces are not very far apart for any shift angle or any regular polygonal shape. For small shifts it is predicted that they are equal, and similar for large shifts, because the shift number is similar for all shapes and all orientations.

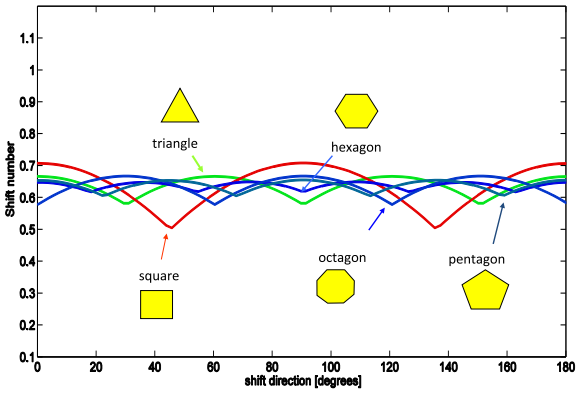

FIG. 3. Shift number as a function of the shift direction for 5 regular polygons.

IV. STAR POLYGONS (REGULAR AND NOT CONVEX)

Consider now the case of star polygons, a class of polygons defined in[24]; and let us examine the case of three polygons: pentagram, hexagram (star of David) and octagram. For small shifts ($x/h < 1/2$) relation (11)) is valid. The case of large shift necessitates calculation of (12) for star polygons. For each type of polygon, two circles can be drawn, passing through the outer vertices and inner vertices. An external r_e and an internal radius r_i can then be defined as functions of the length of the edge s, and, using the same arguments developed in the Appendix B, the restoring force for large shifts can be expressed by

$$F = -\frac{\gamma}{2\sin\frac{\pi}{n}} \sum_i \left| \left[r_e\cos\left(2(i+1)\frac{\pi}{n}\right) - r_i\cos\left(2i\frac{\pi}{n}\right)\right]\sin\alpha + \left[r_e\sin\left(2(i+1)\frac{\pi}{n}\right) - r_i\sin\left(2i\frac{\pi}{n}\right)\right]\cos\alpha \right|, \tag{16}$$

where the radii r_e and r_i are linear functions of s. The shift number showing the isotropic behavior of the chip is shown in figure 4. It varies between 0.55 and 0.65 according to the shift direction.

V. REGULAR POLYGONS WITH REGULAR POLYGONAL CAVITIES

More complex surfaces have also been under scrutiny for capillary self-alignment. Sariola and coworkers have investigated the behavior of a capillary gripper with a cavity in its center[25], and Fukushima and colleagues are studying the alignment of microsystems cover for

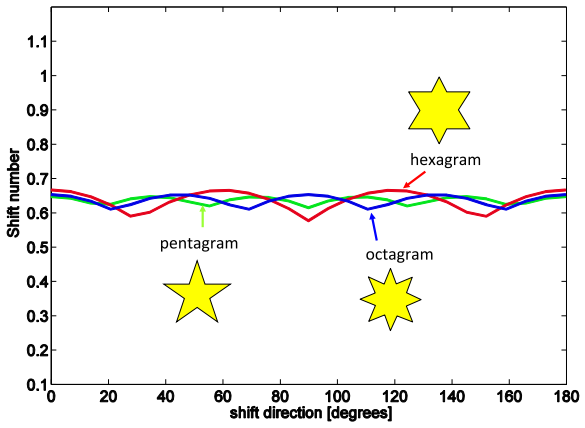

FIG. 4. Shift number for three different star polygons.

packaging[22]. In a general approach, Böhringer and colleagues have shown that couples of composite substrates with hydrophilic and hydrophobic parts will reduce their energy when self-alignment is achieved[26], but even if alignment reduces the system energy, it cannot always be achieved when an energy saddle must be overcome.

In this section, we investigate the shift restoring force for regular polygons – convex or not – with regular polygonal cavities. With the prerequisite of the same free perimeter p, relation (8) for small shift yields

$$F = -\frac{\gamma x}{h}\left(\sum_{i\subset ext} s_i \sin^2\theta_i + \sum_{i\subset int} s_i \sin^2\theta_i\right), \quad (17)$$

where ext refers to the external polygon and int to the internal polygon. This relation is similar to (11). Again, the restoring force at small shift does not depend on the shift direction or on the particular polygonal geometry. On the other hand, relation (9) for large shift, yields

$$F = -\gamma\left(\sum_{i\subset ext} s_i|\sin\theta_i| + \sum_{i\subset int} s_i|\sin\theta_i|\right). \quad (18)$$

Let take the case of a regular polygon with side s and no cavity compared to one with a cavity homothetic to the external polygonal shape, with external side s_{ext} and internal side s_{int}. Assume that both geometries have the same total perimeter p. Then $s_{ext} + s_{int} = s = p/n$. Because the internal and external edges are aligned, the two terms of (18) with summation are equal. Finally, we obtain

$$\begin{aligned} F &= -\gamma(s_{ext} + s_{int})\sum_i |\sin\theta_i| \\ &= -\gamma s \sum_i |\sin\theta_i|. \end{aligned} \quad (19)$$

The theory predicts that the full regular polygon and the polygon with homothetic cavity have the same restoring force, for the same total perimeter.

VI. NUMERICAL APPROACH

The theoretical approach is an approximation since the interfaces have been considered flat. In order to take into account the real shape of the interfaces, we have used the numerical software Surface Evolver[22] to calculate the surface energy for different polygons (fig. 5). First are regular polygons, i.e. convex polygons with $n = 1, 2, \ldots$ edges of same length. We limit ourselves to the equilateral triangle, square, pentagon, hexagon, and octagon. Second, we add the star polygons pentagram, hexagram and octagram. Finally, we consider regular polygons with a regular polygonal cavity: a square with a square cavity, and a triangle with a triangular cavity. All these shapes can be considered "isotropic" as we will see in the following developments. In order to compare with an "anisotropic" shape, we also consider a rectangle of aspect ratio 2 or 1/2 (depending on its position in the coordinates system). Guided by (11), we use the same perimeter $p = 4$ cm in all cases.

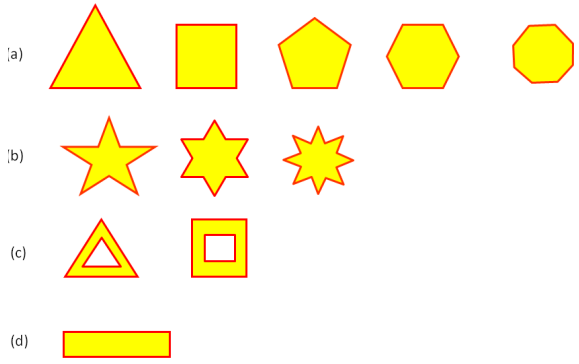

FIG. 5. The different polygons considered in the study: (a) regular, convex polygons; (b) star polygons, (c) regular polygons with regular polygonal cavity, and (d) rectangle of aspect ratio 2.

The numerical protocol is the following: given an initial shift, the interface numerically adjusts to the real physical shape for that fixed shift. The corresponding surface energy is stored in a dedicated file. Then the chip is freed to move incrementally. At each shift increment, the chip is fixed, the interface adjusts and the surface energy again is stored. The relation between the free energy and the shift is then plotted.

In this approach, we consider a uniform perimeter $p = 4.10^{-2}$ m, which corresponds to a square of 1 cm $\times$ 1 cm. We set the liquid volume to $V = Ah$, where A is the surface of the solid wetted by the liquid and h the vertical distance between the two solids. In our case $h \approx 400$ μm (there is a very small deviation due to the curvature of the interface). It is straightforward to show that the surface area of a regular polygon is given by the relation[26]

$$A = \frac{1}{4} n s^2 \cot\frac{\pi}{n}, \quad (20)$$

where n the number of edges, and s the length of an edge.

Figures 6 shows different restoring processes for the different geometrical shapes considered.

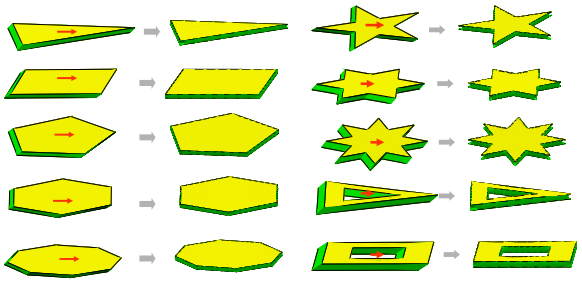

FIG. 6. Capillary self-alignment for star polygons and polygons with cavities, obtained with Surface Evolver.

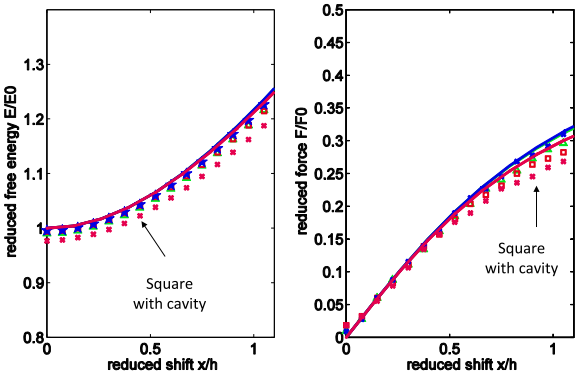

FIG. 7. Comparison between theory (continuous lines) and numerical model (dotted lines) for four different polygonal shapes with same perimeter: equilateral triangle, square, pentagon and square with cavity. The references E_0 for energy and F_0 for the force are respectively $E_0 = \gamma hp$ and $F_0 = \gamma p$.

VII. RESULTS

In this section, a comparison between the theoretical and numerical approaches is presented first. Then the influence of the shift direction and chip shape on the free energy and on the restoring force is investigated. It is recalled that the restoring force is given by

$$F = -\frac{\delta E}{\delta x}, \tag{21}$$

where E denotes the free energy and x the shift.

A. Comparison between theoretical and numerical results

A comparison between theoretical and numerical results for a 0° shift is shown in figure 7, for four different polygonal shapes (triangle, square, pentagon and square with cavity). The agreement between theory and numerical model is good – which signifies that the hypothesis of flat surfaces is not too far from the reality – except maybe for the case of the square with a square cavity. In this case, the theory predicts the same restoring force as for the square. The discrepancy comes from the number of additional corners of the square with cavity. The real free surface becomes smaller for each additional corner, as is shown in figure 8.

The agreement also depends on the height h of the liquid layer. A large value of h would certainly increase the influence of the curvature of the interfaces. In the present case, the aspect ratio $\epsilon = 2h/p$ of the thickness of the liquid layer and half the free perimeter is only 0.02. In the industrial process, a still smaller ratio is expected.

The preceding observation is still more acute in the case of star polygons: the presence of sharp angles and reentrant angles decreases the liquid interfacial area, and reduces the restoring force (fig. 9).

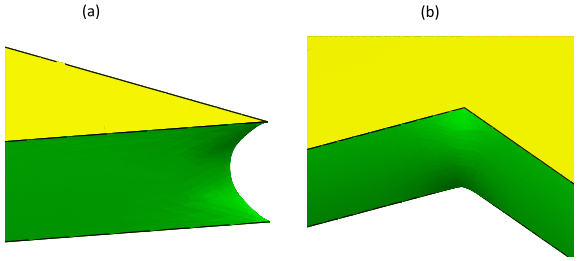

FIG. 8. View of the liquid interface in sharp or reentrant corners (Evolver).

In conclusion, the theory slightly overestimates the magnitude of the restoring force; but as the thickness of the liquid layer will be smaller in the real process, the difference between theory and numerical model is expected to be less than that shown in figure 9.

B. Influence of shift direction - isotropicty and anisotropicity

We analyze now the restoring force as a function of the shift direction. In section II it has been found that for regular polygonal shapes, theory predict an independence of the shift-restoring force for small shifts ($x/h < 1/2$), and a moderate dependence for large shifts ($x/h > 1$). In this section we use the Evolver to check these theoretical results.

Consider a square chip, and different directions of shift: α= 0, 30, 45, 60, 90, 135 and 180 degrees. A plot of the different restoring forces based on the general relation (7) is shown in figure 10. It is observed that when x/h is smaller than approximately $1/2$, the restoring forces are all equal, as expected from the theory. The same results can be obtained for all the regular polygonal shapes. We

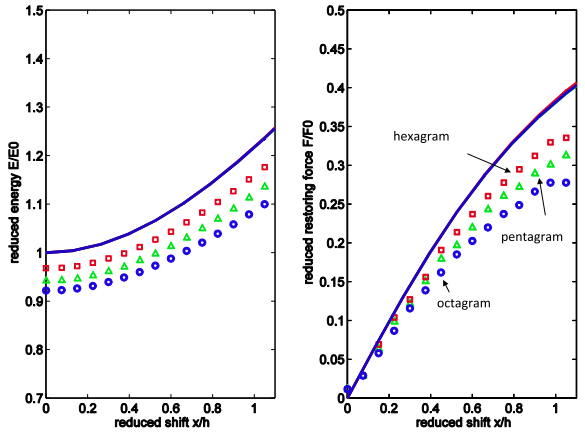

FIG. 9. Comparison between theory and numerical approach for star polygons (of same perimeter). Continuous lines correspond to the theory and dotted lines to Evolver calculations.

deduce that when x/h is less than $1/2$, the shift direction has no influence on the close range restoring forces for "isotropic" chips.

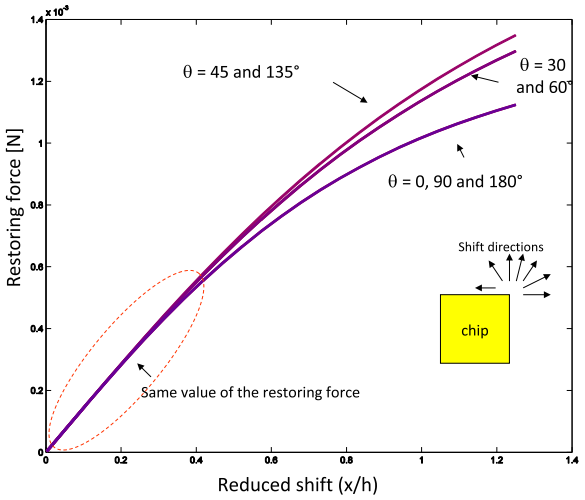

FIG. 10. Restoring forces as a function of the shift magnitude and direction (from Evolver).

On the other hand, this is not the case with a "non-isotropic" polygonal shape, such as the rectangle. In figure 11, the shift number has been plotted as a function of the shift direction. Isotropic behavior is characterized by a shift number Sf of 0.62 corresponding to the octagon (regular polygon with many edges). An approximate isotropic situation occurs for shift numbers comprised between 0.55 and 0.7. The square can be considered as the limit. The shift number for a rectangle of aspect ratio 2 varies between 0.3 and 0.75, which indicates an anisotropic behavior.

Note that, from Appendix A, the anisotropy is characterized by the ratio between the maximum and minimum

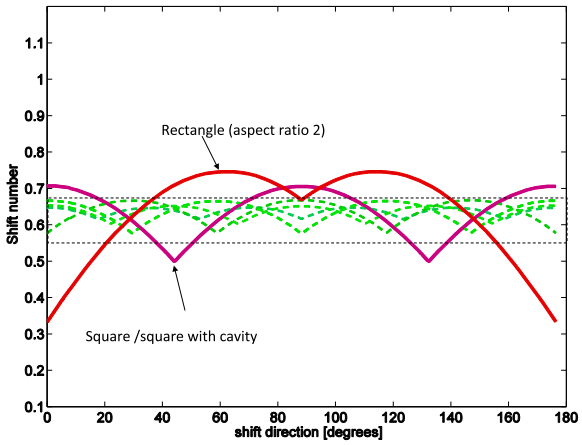

FIG. 11. Shift number as a function of the shift direction. The green curves correspond to the equilateral triangle, pentagon, hexagon and octagon. Their behavior is nearly isotropic. The magenta curve corresponds to the square shape, at the limit of isotropic behavior, and the rectangle (red line) is fully anisotropic.

cross lengths of the polygonal chip. In the case of a square $L_{max}/L_{min} = \sqrt{2}$. More generally, it can be shown for regular polygons, that $L_{max}/L_{min} = 1/\cos\frac{\pi}{n}$.

C. Influence of polygonal shape

Let us now consider the different polygonal shapes of figure 5. Free surface energies are plotted in figure 12 as a function of a shift in the direction of the x-axis. From the figure, we deduce that all "isotropic" shapes – regular polygons, with a regular polygonal cavity, and star polygons – have a similar free surface energy, while the surface energy of the "anisotropic" rectangle notably differs from the other "isotropic" shapes. Using (7), the same conclusion can be drawn for the shift restoring force, as shown in figure 13.

D. Restoring force for small shifts

A perfect alignment is obtained when the force at small shift is sufficiently large; this can be characterized by determining the value of the derivative of the restoring force $\Delta = dF/dx_{|x=0}$ at the origin. The value of Δ has been obtained numerically from the Evolver values of figure 13. In figure 14, we have plotted the value of Δ for different polygonal geometries (with same free perimeter p) for very small shifts. For all regular polygonal geometries, the value of Δ converges towards the theoretical value $\Delta = \gamma p/2h = \gamma/\epsilon$. On the other hand, the value of Δ for anisotropic geometries (here a rectangle) differs considerably from the theoretical results.

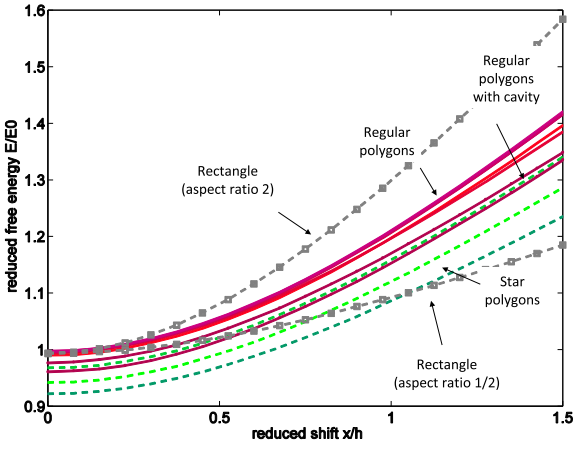

FIG. 12. Free energy vs. shift for the different polygonal shapes obtained with the Surface Evolver.

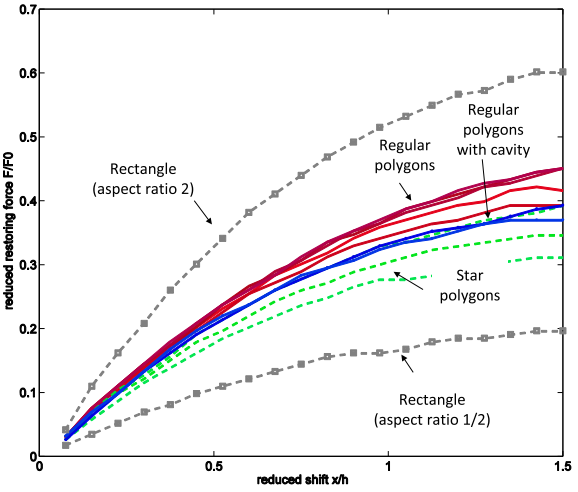

FIG. 13. Restoring force versus shift for different polygonal shapes with same free perimeter: The restoring forces are similar except for the anisotropic rectangle. Values obtained with the Evolver.

VIII. APPLICATION TO MICROSYSTEM PACKAGING

In this section, we investigate the shift restoring force in the geometry of a square microsystem where vias (channels) are opened on two opposite sides, as proposed by Fukushima and colleagues in[21]. Closed square shapes (with square cavities) have been investigated above, and we focus here on the anisotropy induced by the vias (fig. 15). In this particular case, the width of the channels piercing the square is set to 1/10 of the external edge, and the cavity dimension is half that of the external dimension. In contrast with the preceding sections, we consider the same external dimensions of the square polygons in both cases, regardless of the difference between the free perimeters.

Figure 16 shows the restoring force as a function of

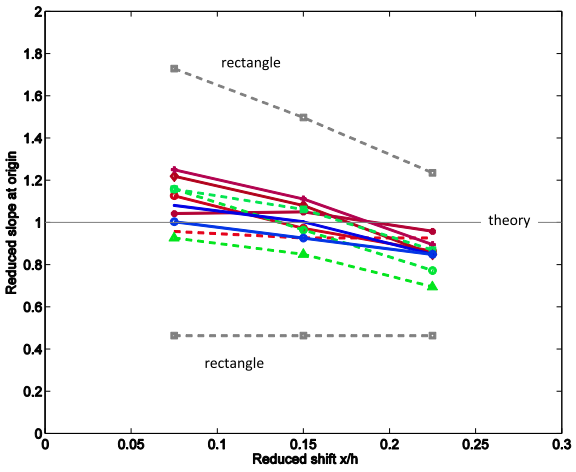

FIG. 14. Value of dF/dx at small shifts: all the regular polygons converge to the analytical value, while the anisotropic rectangular shape differs notably from this value (from Evolver).

the shift for the square chip (with square cavity) and for the cavity-chip along two perpendicular directions of the shift: first, the direction of the channels – x-direction – and second the direction perpendicular to the channels – y-direction. The anisotropy induced by the channels clearly appears in the figure.

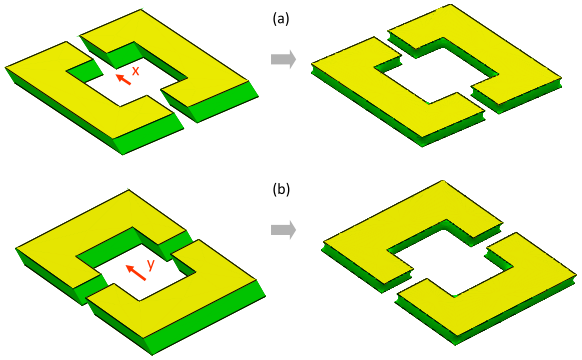

FIG. 15. Alignment of a square microsystem cover after a x-shift (a), and a y-shift (b).

In the same figure, we have also plotted two "modified" curves: the first one corresponds to the value of the force in the x-direction decreased by the missing interfacial area corresponding to the channel openings. If s_{ext} denotes the (external) square edge, and w the width of the channels, we have

$$\frac{F_{microsystem}}{F_{square}} = \frac{2s_{ext} - 4w}{2s_{ext}} = 1 - 2\frac{w}{s_{ext}}. \qquad (22)$$

Conversely, in the case of a y-shift, the value of the restor-

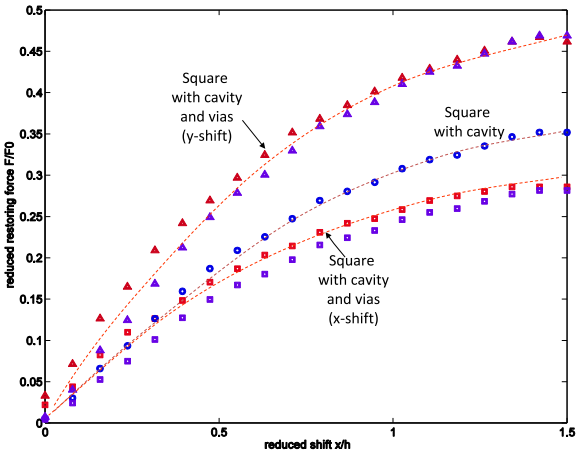

FIG. 16. Shift restoring force: comparison between a square (with cavity) and a square (with cavity) pierced by two channels. The two channels induce anisotropy of the restoring forces. Calculation performed with Surface Evolver. The two additional curves are obtained from the square (with cavity) curve multiply by the corrective factors given by (22) and (23).

ing force is increased by

$$\frac{F_{microsystem}}{F_{square}} = \frac{2s_{ext} + 2s_{int} + 2(s_{ext} - s_{int})}{2s_{ext} + 2s_{int}} = 2\frac{s_{ext}}{s_{ext} + s_{int}}. \quad (23)$$

Using the values $w = s_{ext}/10$ and $s_{ext} = 2s_{int}$, we find the correction coefficients 4/5 and 4/3, which reproduce well the restoring force for a full (no channels) square with cavity. Hence, the restoring force at small shift can be approximated by

$$f = \frac{F}{\gamma p} = -\frac{x}{2h}\left(1 - 2\frac{w}{s_{ext}}\right) \quad (24)$$

for a shift along the channel axis, and

$$f = \frac{F}{\gamma p} = -\frac{x}{2h}\left(2\frac{s_{ext}}{s_{ext} + s_{int}}\right) \quad (25)$$

for a shift perpendicular to the channel axis. Relations (24) and (25) constitute the two limits for the restoring force at small shift for the pierced geometry considered here. The shift number is comprised between the values.

$$\frac{x}{2h}\left(1 - 2\frac{w}{s_{ext}}\right) < Sf < \frac{x}{2h}\left(2\frac{s_{ext}}{s_{ext} + s_{int}}\right). \quad (26)$$

IX. CONCLUSIONS AND PERSPECTIVES

In this work, an approximate closed form of the shift-restoring force has been derived from the assumption of flat interfaces for many different regular polygonal shapes. It has been shown that this analytical expression agrees well with the more detailed value produced by a numerical approach with the numerical software Surface Evolver. An interesting observation is that, for small shifts, the restoring force does not depend on the shift direction or on the polygonal shape. The restoring force is simply proportional to the surface tension, to the free perimeter and to the magnitude of the shift.

A non-dimensional number, the shift number, has been defined that characterizes the non-dimensional shift-restoring force, and the isotropicity of the system (for large shifts), i.e. the independence of the restoring force to the shift direction.

An extended expression of the shift-restoring force at close range has been derived for chips with cavity pierced by connection vias (microchannels), similar to that used for packaging microsystems. This extended relation has again been verified by a numerical approach.

So far, only the effect of the shift has been investigated. Twist, tilt and roll restoring torques are still to be investigated, in order to have a complete assessment of the capillary effect on different polygonal chips.

Appendix A: RESTORING FORCES FOR LARGE SHIFTS FOR ANY POLYGON

The force at large shift given by equation (9)

$$F = -\text{sign}(x)\gamma \sum_i s_i |\sin\theta_i| \quad (A1)$$

has a geometrical significance. In figure 17, the projections of the edges s_i on the direction perpendicular to the shift show that

$$\sum_i s_i |\sin\theta_i| = \frac{L_\perp}{2}. \quad (A2)$$

The restoring force at large shift is then

$$F = -\text{sign}(x)\gamma\frac{L_\perp}{2}. \quad (A3)$$

The magnitude of the restoring force is then comprised between the minimum and maximum cross lengths L_{min} and L_{max} (fig. 17).

Appendix B: RESTORING FORCES FOR LARGE SHIFTS

For a regular polygon with n edges of length s and free perimeter p, the following relation holds:

$$p = ns. \quad (B1)$$

Using trigonometrical calculation, we find the value of the circumscribed circle to be

$$r = \frac{n}{2\sin\frac{\pi}{n}}. \quad (B2)$$

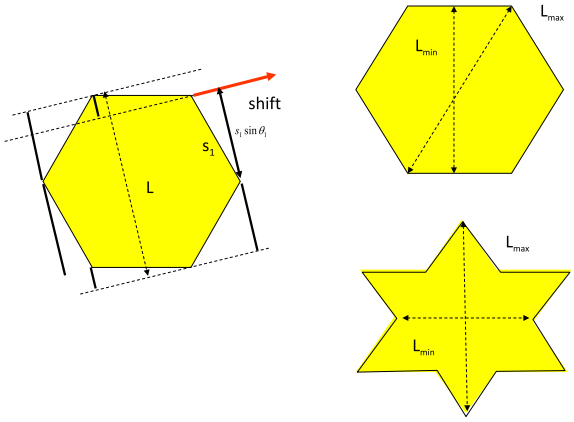

FIG. 17. Left: projections on the direction perpendicular to the shift; right: the two extrema for a hexagon and a hexagram.

Incidentally, the surface area of the solid wetted by the liquid can be expressed as a function of the perimeter p and the number of edges n:

$$A = \frac{1}{4} n s^2 \cot\frac{\pi}{n} = \frac{1}{4} p^2 \frac{1}{n} \cot\frac{\pi}{n}. \tag{B3}$$

The coordinates of the polygon vertices are

$$S_i = r\left[\cos\left(2i\frac{\pi}{n}\right), \sin\left(2i\frac{\pi}{n}\right)\right], \tag{B4}$$

where i is the vertex index. The oriented vector edges are then

$$\vec{s_i} = r\left[\cos\left(2(i+1)\frac{\pi}{n}\right) - \cos\left(2i\frac{\pi}{n}\right), \sin\left(2(i+1)\frac{\pi}{n}\right) - \sin\left(2i\frac{\pi}{n}\right)\right] \tag{B5}$$

Let us assume that the shift direction is the unit vector defined by its polar angle α,

$$\vec{k} = \{\cos\alpha, \sin\alpha\}. \tag{B6}$$

The cross-product between $\vec{s_i}$ and $\vec{k}$ produces the value of $\sin\theta_i$:

$$\sin\theta_i = \frac{\vec{s_i}}{\parallel s_i \parallel} \times \vec{k}. \tag{B7}$$

We finally find the expression

$$\sin\theta_i = \frac{1}{2n\sin\frac{\pi}{n}} \left\{ \left[\cos\left(2(i+1)\frac{\pi}{n}\right) - \cos\left(2i\frac{\pi}{n}\right)\right] \sin\alpha - \left[\sin\left(2(i+1)\frac{\pi}{n}\right) - \sin\left(2i\frac{\pi}{n}\right)\right] \cos\alpha \right\}. \tag{B8}$$

[1] T. Fukushima, T. Tanaka, M. Koyanagi, "3D System Integration Technology and 3D Systems," *Advanced Metallization Conference Proceedings*, pp. 479-485, 2009.

[2] J. Yeh and J. S. Smith, "Fluidic self-assembly for the integration of GaAs light emitting diodes on Si substrates," *IEEE Photon. Technol. Lett.*, **6**, p. 706, 1994.

[3] Wei Zheng, H. O. Jacobs, "Fabrication of multicomponent microsystems by directed three-dimensional self-assembly," *Adv. Funct. Mater.* **15**, p. 732, 2005.

[4] M. Mastrangeli, S. Abbasi, C. Varel, C. Van Hoof, J-P. Celis and K. F. Bohringer, "Self-assembly from milli- to nanoscales: methods and applications," *J. Micromech. Microeng.* **19**, p. 083001, 2009.

[5] J. Berthier, K. Brakke, F. Grossi, L. Sanchez and L. Di Cioccio, "Self-alignment of silicon chips on wafers: A capillary approach," *JAP* **108**, p. 054905, 2010.

[6] P. Lambert, M. Mastrangeli, J. -B. Valsamis, G. Degrez, "Spectral analysis and experimental study of lateral capillary dynamics for flip-chip applications," *Microfluid Nanofluid.*, **9**, pp. 797–807, 2010.

[7] M. Mastrangeli, S. Abbasi, C. Varel, C. Van Hoof J-P. Celis and K. F. Bohringer, "Self-assembly from milli- to nanoscales: methods and applications," *J. Micromech. Microeng.*, **19**, p. 083001, 2009.

[8] Bo Chang, V. Sariola, S. Aura, R.H.A. Ras, M. Klonner, H. Lipsanen, Quan Zhou, "Capillary-driven self-assembly of microchips on oleophilic/oleophobic patterned surface using adhesive droplet in ambient air," *APL* **99**, p. 034104, 2011.

[9] J. Berthier, K. Brakke. *The physics of microdrops.* Scrivener-Wiley publishing, 2012.

[10] T. Fukushima, T. Tanaka, and M. Koyanagi, Proceedings of the Advanced Metallization Conference, pp 479–485, 2009.

[11] W. Zheng, H. O. Jacobs, "Fabrication of multicomponent microsystems by directed three-dimensional self-assembly," *Adv. Funct. Mater.*, **15**, p. 732, 2005.

[12] H. Moriceau, F. Rieutord, F. Fournel, Y. Le Tiec, L. Di Cioccio, C. Morales, A. M. Charvet and C. Deguet , "Overview of recent direct wafer bonding advances and applications," *Adv. Nat. Sci.: Nanosci. Nanotechnol.* **1**, p. 043004, 2010.

[13] Q. Y. Tong and U. Gösele. *Semiconductor Wafer Bonding.* Wiley, Hoboken, NJ, 1999.

[14] J. Berthier, K. Brakke, S. Mermoz, L. Sanchez, C. Frétigny, L. Di Cioccio, "Self-alignment of Silicon Chips on Wafers: a Numerical Investigation of the Effect of Spreading and Wetting," *Sensors & Transducers Journal* **13**, pp. 44-52, 2011.

[15] S. Mermoz, L. Sanchez, L. Di Cioccio, J. Berthier, E. Deloffre and C. Fretigny, "Impact of Containment and Deposition Method on Sub-Micron Chip-to-Wafer Self-Assembly Yield," *Proceedings of the 3DIC Conference*, Osaka, Japon, January 31-February 2, 2011.

[16] Sang Hwui Lee, Kuan-Neng Chen, J. Jian-Qiang Lu, "Wafer-to-Wafer Alignment for Three-Dimensional Integration: A Review," *J. Microelec. Syst.* **20**(4), p.885, 2011.

[17] M. Boncheva, D. A. Bruzewicz, and G. M. Whitesides, "Millimeter-scale self-assembly and its applications," *Pure Appl. Chem. 75* (5), pp. 621–630, 2003.

[18] R. J. Knuesel and H. O. Jacobs, "Self-assembly of microscopic chiplets at a liquid-liquid-solid interface forming a flexible segmented monocrystalline solar cell ," *PNAS* **107**(3), p. 993, 2010.

[19] A. Avital and E. Zussman, "Fluidic Assembly of Optical Components," *IEEE Trans. Adv. Packag* **29**(4), p.719, 2006.

[20] X. J. Zhang, C. C. Chen, R. W. Bernstein, S. Zappe, M. P. Scott, and O. Solgaard, "Microoptical Characterization and Modeling of Positioning Forces on Drosophila Embryos Self-Assembled in Two-Dimensional Arrays," *J.Microelectromech. S.* **14**(5), p. 1187, 2005.

[21] S. A. Stauth, B. A. Parviz, "Self-assembled single-crystal silicon circuits on plastic," *PNAS* **103**(38), p. 13922, 2006.

[22] T. Fukushima, T. Konno, E. Iwata, R. Kobayashi, T. Kojima, M. Murugesan, J-C Bea, K-W Lee, T. Tanaka, and M. Koyanagi, "Self-Assembly of Chip-Size Components with Cavity Structures: High-Precision Alignment and Direct Bonding without Thermal Compression for Hetero Integration," *Micromachine* **2**, pp.49-68, 2011.

[23] K. Brakke, "The Surface Evolver," *Experimental Mathematics* **1**(2), pp. 141-165, 1992.

[24] http://www.mathworld.wolfram.com/StarPolygon.html.
[25] V. Sariola, V. Liimatainen, T. Tolonen, R. Udd, and Quan Zhou, "Silicon capillary gripper with self-alignment capability," *2011 IEEE International Conference on Robotics and Automation Shanghai International Conference Center*; May 9-13, 2011, Shanghai, China.
[26] K.F. Böhringer, U. Srinivasan, R.T. Howe, "Modeling of capillary forces and binding sites for fluidic self-assembly," *Int. Conf. Micro Electro Mechanical Systems*, 2001.
[27] http://www.en.wikipedia.org/wiki/regular_polygon.